

Organic & Biomolecular Chemistry

Accepted Manuscript



This is an *Accepted Manuscript*, which has been through the Royal Society of Chemistry peer review process and has been accepted for publication.

Accepted Manuscripts are published online shortly after acceptance, before technical editing, formatting and proof reading. Using this free service, authors can make their results available to the community, in citable form, before we publish the edited article. We will replace this *Accepted Manuscript* with the edited and formatted *Advance Article* as soon as it is available.

You can find more information about *Accepted Manuscripts* in the [Information for Authors](#).

Please note that technical editing may introduce minor changes to the text and/or graphics, which may alter content. The journal's standard [Terms & Conditions](#) and the [Ethical guidelines](#) still apply. In no event shall the Royal Society of Chemistry be held responsible for any errors or omissions in this *Accepted Manuscript* or any consequences arising from the use of any information it contains.

Homocoupling versus Reduction of Radicals: An Experimental and Theoretical Study of Ti(III)-mediated Deoxygenation of Activated Alcohols

Cite this: DOI: 10.1039/x0xx00000x

Received 00th January 2012,
Accepted 00th January 2012

DOI: 10.1039/x0xx00000x

www.rsc.org/

Consuelo Prieto,^a José A. González Delgado,^a Jesús F. Arteaga,^{*b} Martín Jaraíz,^{*c} José L. López-Pérez^d and Alejandro F. Barrero^a

Abstract. A detailed experimental and theoretical study corroborates that the reductive deoxygenation of activated (allylic or benzylic) alcohols with excess Ti(III) proceeds via allyl(benzyl)-radical and allyl(benzyl)-Ti, which is protonated, regioselectively in the case of allylic derivatives. The H atom of the newly formed C–H bond in the product originates from the –OH group of the starting material. Deoxygenation of lithium alkoxides or alcohols by using 1.0 mol of Ti(III) leads to the corresponding dimerization product in good yield. An excellent agreement with the experimental data was obtained by using a reaction kinetics simulator to discriminate between competing reactions.

Introduction

Nugent's reagent (Cp_2TiCl , Fig. 1) is an excellent mediator in many reactions of synthetic interest.¹

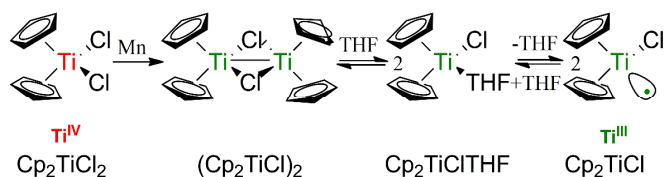


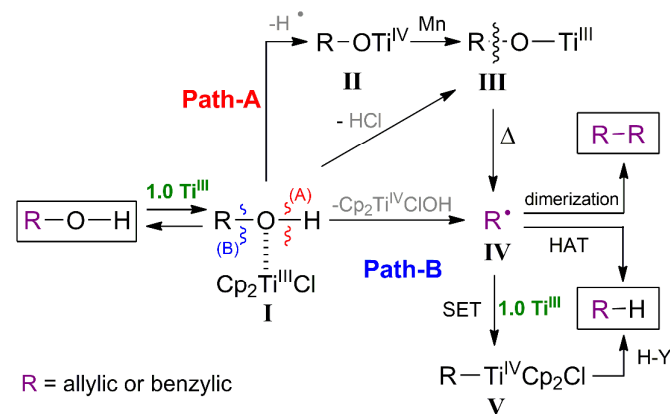
Fig. 1. Preparation of Cp_2TiCl by reaction of Cp_2TiCl_2 and Mn.

Initially it behaves as a Lewis acid and forms complexes with different functional groups that contain heteroatoms with non-bonding electron pairs. Thus, an electron transfer takes place from Ti(III), which leads to the homolytic cleavage of X–Ti bond and subsequently to a C-centred radical. Various synthetic applications deriving from the reactivity of these radicals, including allylic and benzylic radicals, are already known.² For example, it has recently been reported that activated alcohols give rise to deoxygenation-reduction reactions via radicals in the presence of catalytic quantities or an excess of Ti(III).³ Furthermore, alcohol derivatives such as allylic carbonates and acetates are reduced by the Pd(0)/Ti(III) system and H_2O .⁴ Ti(III) and Zr(IV)/Mn have also been showed to enable the efficient homocoupling of activated halogenated derivatives.⁵ Homocoupling of vinyl epoxides under catalytic conditions, and reductions with an excess of Ti(III) have been reported as well.^{6,7} The underlying mechanisms have been interpreted in terms of radical dimerization, H-atom transfer (HAT) processes, couplings via organo-Ti, and the protonation of organo-

Ti intermediates. However, much uncertainty regarding the detailed mechanistic pathways persists. Herein, we describe the results of a detailed experimental and theoretical study with the aim to clarify the mechanistic nature of the Ti(III)-mediated deoxygenation of activated alcohols. We also test the possibility of dimerizing activated alcohols by using Ti(III).

Results and discussion

Besides the reported³ homolysis of the C–O bond through the formation of Ti-complex **I** (Scheme 1, Path-B), we analysed an alternative route involving the homolysis of the O–H bond in **I** (Scheme 1, Path-A).



Scheme 1. Proposed mechanisms for the deoxygenation of activated alcohols

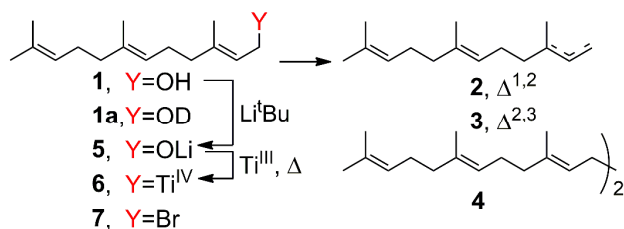
This path produces the Ti(IV) alkoxide **II**, which is reduced with Mn excess to the Ti(III) alkoxide **III**. The latter evolves upon heating to the radical **IV** and titanocene oxide. Radical **IV** is the

common key intermediate along the two pathways towards the final products (R–H, Scheme 1) of the deoxygenation-reduction reaction, with two possibilities of trapping the H atom: (i) a direct HAT process, or (ii) a two-step transformation, with Cp_2TiCl (SET) forming first an alkyl or benzyl–Ti species (V) (Scheme 1, Path–B) which can be protonated subsequently by Brønsted acids H–Y present in the medium or in the work-up.⁸ Competitively radical IV could dimerize to produce homocoupling products R–R (Scheme 1 and Scheme 4).

Experimental results

With the aim of verifying experimentally what type of mechanisms are involved we tried first to identify the source of the H atom that causes the reduction. To that end, we ran the first reaction with farnesol (**1**, Table 1) excess Cp_2TiCl_2 and Mn (powder 99,9%) using reported experimental conditions,³ adding in the work-up D_2O instead of H_2O . However, no deuteration in the reduction products (**2–3**) was observed (Table 1, entry 1). Neither did we observe deuteration when we used deuterated THF as solvent (Table 1, entry 2).

Table 1. Ti(III)-mediated reduction-homocoupling of farnesol (**1**)

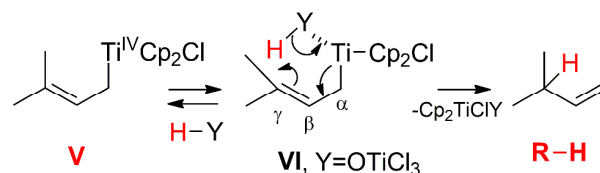


Entry ^a	Cp_2TiCl_2 (equiv.)	Mn (equiv.)	Time (hours)	Product, Yield (%)			
				1	2	3	4
1	2.0	8.0	2	–	78	8	9
2 ^b	2.0	8.0	2	–	75	7	11
3 ^c	2.0	8.0	5	–	87 ^d	10	–
4 ^e	–	–	4	–	41	41	–
5 ^{f,g}	1.0	1.0	0.6	–	–	–	48
6 ^h	1.0	0.5	10	–	4	–	67
7	1.0	8.0	6	15	42	3	23
8	1.0	1.0	4	–	24	4	36
9	1.0	0.5	4	2	10	<1	45

^aGeneral experimental conditions: **1** as starting material, 0.2 M THF and THF reflux (oil bath at 100 °C). ^bDeuterated THF was employed. ^c**1a** was used. ^d80% deuteration was found. ^eExperiment run with **7** as starting material and reacted with Bu_3SnH . ^fHCl was removed under Ar flow. ^gOil bath at 150 °C. ^hReaction via **5**.

Then, we prepared deuterio-farnesol (**1a**) which gave an 87% yield of **2** with 80% deuteration (Table 1, entry 3). Besides under certain experimental conditions, for example by increasing the heat-transfer rate or by subjecting the reaction mixture to a high Ar flow, HCl gas (potential source of H^+ at the reaction media) is seen to be given off and its elimination from the reaction media led exclusively to the formation of dimer (Table 1, entry 5). These initial experiments suggest that the H of the reduction comes from the –OH group of the

starting material.

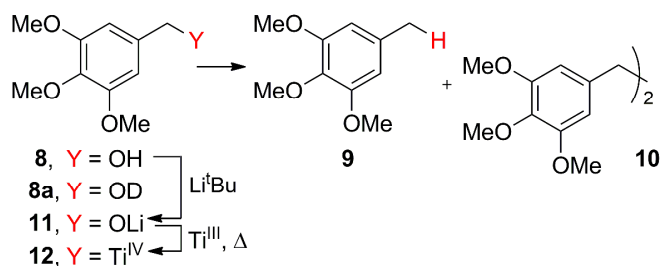


Scheme 2. Mechanism of selective γ -position protonation

To clarify what class of mechanism may be responsible for introducing the H atom into the final product we looked at the regiochemistry of the reaction involving allylic substrates: under the standard conditions the least-substituted olefin was formed with good regioselectivity (Table 1, entries 1–3). This indicates that the regio-modulated entry of the H takes place at the most substituted C.³ Within this context, the dehalogenation-reduction of halogenated derivatives via the use of Bu_3SnH constitutes a good example of HAT-mediated reduction. Consequently, when we reacted farnesyl bromide (**7**) with Bu_3SnH no regioselectivity was observed and a 1:1 mixture of compounds **2** and **3** (82% overall yield) was obtained as the result of allylic radical scavenging by Bu_3SnH (Table 1, entry 4).

These results rule out any HAT-type process during the reduction, and reinforce the hypothesis of a mechanism via alkyl–Ti (**V**) and protonation in the reaction media (thus an H^+ source is required). According to Scheme 2, **V** must place the bulky Cp_2TiCl mainly at the C–1 position, which should then give rise to direct protonation probably by Cp_2TiClOH at C–1, thus leading to a double bond ($\Delta^{2,3}$). In order to justify the observed highly regioselective formation of the double bond ($\Delta^{1,2}$), we propose that the Ti atom of **V** acts as Lewis acid before protonation occurs and coordinates a Brønsted acid from the medium originating the Ti–complex **VI** (Schemes 2 and 4). Thus, protonation can undergo intramolecularly from **VI** via a 6-membered cyclic transition state, preferably in the γ -position (Scheme 2). These results suggest that the H atom of the reduction comes from the starting –OH group and that 2.0 mol of Ti(III) are required if Cp_2TiClOH is the protonating agent. Consequently, when the H atom of the –OH group of **1** was eliminated by using Li derivative **5**, the dimer **4** was obtained as main product by using 1.0 equiv. of Ti(III) (Table 1, entry 6). Furthermore, it is well known that the dimerization rate of allylic radicals is higher if their molar concentration is increased. Thus the reaction of **1** with only 1.0 equiv. of Ti(III) and various quantities of Mn led to a higher proportion of **4** in comparison to **2** and **3** (Table 1, entries 7–9).

As with allylic compounds, deoxygenation–reduction and dimerization products were obtained when primary benzylic alcohols reacted with excess Ti(III). Thus, if 3,4,5-trimethoxybenzyl alcohol (**8**) is reacted under standard conditions up to 90% yield of toluene derivative (**9**) is obtained, with the 5% yield of the starting material (**8**) being recovered (Table 2, entry 1). If smaller proportions of Ti and Mn as 1.0 equiv. of Ti(IV) and 1.0 or 0.5 equiv. of Mn are used, the yield of **9** decreases to 80% and 46% respectively (Table 2, entries 3–4). When the molar concentration was increased to 0.8 M a 14% yield of dibenzyl derivative (**10**) is obtained, that is, the dimerization process competes with the homocoupling one (Table 2, entry 5). On the other hand, the reaction of lithium alcoxide (**11**) obtained from **8** with 1.2 equiv. of Ti(III) also increased the proportion of dimer (**10**) to 60% as opposed to 7% of reduction product (**9**) (Table 2, entry 6).

Table 2. Ti(III)-mediated reduction-homocoupling of 3,4,5-trimethoxybenzyl alcohol (**8**)

Entry ^a	Cp ₂ TiCl ₂ (equiv.)	Mn (equiv.)	Time (hours)	Product, Yield (%)		
				8	9	10
1	2.0	8.0	1	5	91	–
2 ^b	2.0	8.0	1	3	88 ^c	–
3	2.0	1.0	2	15	80	–
4	1.0	0.5	6	50	46	–
5 ^d	1.0	0.5	1	38	40	14
6 ^e	1.2	0.6	24	19	7	60

^aGeneral experimental conditions: **8** as starting material, 0.2 M THF and THF reflux (oil bath at 100 °C). ^b**8a** was used. ^c82% deuteration was found. ^d0.8 M of molar concentration for this experiment. ^eReaction via **11** and subsequent refluxing.

Theoretical results

Theoretical calculations with Gaussian⁹ have been undertaken to corroborate the above outlined mechanistic proposal. We performed the calculations of **1b** (R = dimethylallyl in Scheme 1) as representative species of the study with DFT using the B3LYP/6-31+G(d,p)^{10,11} as recommended method for reaction barrier calculations in general (see SI, section 3.5. for a comparative study on the performance of several computation models). To perform the calculations of the large number of reactions involved (Table 3) with this accurate method we simplified the model, using TiCl₃ instead of Nugent's reagent (Cp₂TiCl) which is employed in experimental studies. This is mainly due both to the complexity of simulating some intermediates possessing two titanocene moieties but also to their increasing computational cost. Experimentally it is well established that both compounds have shown similar chemical behaviour.¹² We have verified that this similarity is also true from the theoretical approach, by comparing the results obtained with Cp₂TiCl for a similar radical system,¹³ and the predictions that we obtain with TiCl₃ (See SI, section 3.6). We found that the species of type **II** (R–OTi^{IV}, Scheme 1) resulted in a much higher energy than the initial complex **I**. In addition, when the H bonded to the O atom is abstracted through a relaxed scan, the transition state¹⁴ is a saddle-point which shows an activation energy (AE) of 28.9 Kcal/mol. This AE is considerably higher than that of the C–O homolysis (12.2 Kcal/mol; r05 in Table 3 and Scheme 4; in SI: 3.4.6). Hence, the latter proposed pathway (Scheme 1, Path–B) is inferred to be the mechanism of deoxygenation via the radical R[•] (**IV** in Scheme 1).

Table 3. Reaction set and energy barriers (Kcal/mol) in the reaction of dimethylallyl alcohol (**1b**) and Ti(III).

	Reaction ^a	Barrier	G ^b	Opt ^c
r00	Mn + 2 TiCl ₄ → MnCl ₂ + 2 TiCl ₃	b00	–	17.8
r01	TiCl ₃ + THF ↔ TiCl ₃ THF	b01	0.0	0.0
r02	2 TiCl ₃ ↔ (TiCl ₃) ₂	b02	0.0	0.0
r03	R–OH + TiCl ₃ THF ↔ TiCl ₃ ROH + THF	b03	12.9	12.3
r04	R–OH + TiCl ₃ → TiCl ₃ ROH	b04	0.0	0.0
r05	TiCl ₃ ROH → R [•] + TiCl ₃ OH	b05	12.2	12.5
r06	2 R [•] → R–R	b06	0.0	0.0
r07	R [•] + TiCl ₃ → TiCl ₃ R	b07	0.0	0.0
r08	R [•] + TiCl ₃ THF ↔ TiCl ₃ R + THF	b08	0.0	0.0
r09	TiCl ₃ R + TiCl ₃ OH → R–H + (TiCl ₃) ₂ O	b09	10.0	10.0
r10	TiCl ₃ R + HCl → R–H + TiCl ₄	b10	12.9	12.9
r11	TiCl ₃ OH + TiCl ₃ ↔ (TiCl ₃) ₂ OH	b11	0.0	0.0
r12	TiCl ₃ OH + TiCl ₃ THF ↔ (TiCl ₃) ₂ OH + THF	b12	0.0	0.0
r13	(TiCl ₃) ₂ OH ↔ HCl + Ti ₂ Cl ₅ O	b13	10.3	8.6
		b13r ^d	1.4	1.0

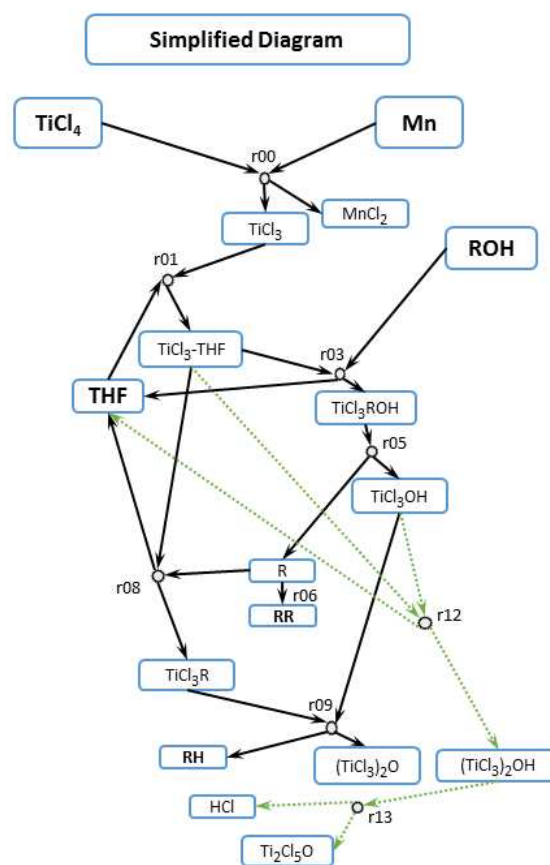
^aR = dimethylallyl. ^bGaussian values B3LYP/6-31+G(d,p) scrf = (smd, solvent = THF) // B3LYP/6-31+G(d,p). ^cValues optimized with Copasi. ^dData corresponding to reverse process.

Kinetics Modelling Simulation

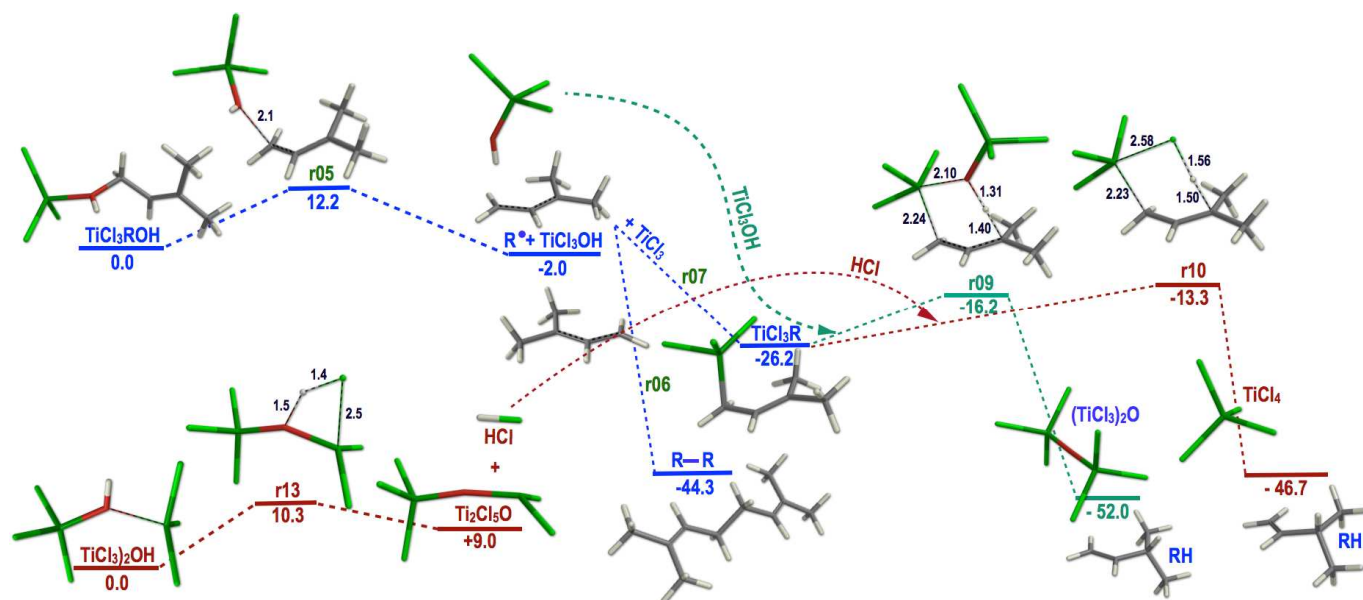
To study pathway B in detail the reaction set listed in Table 3, simplified Scheme 3¹⁵ and Scheme 4 were modelled computationally with the kinetics modelling simulator Copasi,^{16,17} taking into account explicitly the influence of the solvent molecules.

According to the simulation (using the barriers calculated first with Gaussian and then optimized with Copasi to better fit the experimental data) the overall reactions proceed as follows. Initially there are only TiCl₄ and Mn in the THF medium. Each TiCl₃ radical generated (Table 3, reaction r00 with barrier b00 estimated to fit the experimental time) is immediately solvated with THF (r01) instead of forming its dimer through the competing r02, because of the concentration of THF is much higher than that of the generated TiCl₃.¹⁵ (TiCl₃)₂ has been proposed to be one of the major reducing agents in THF,¹⁸ but the kinetics results presented herein establish that the reducing agent is the competing solvated species (TiCl₃THF) which, is in a much higher concentration than the dimer. Subsequently, R–OH is added and forms the TiCl₃ROH complex **I** (through r03 rather than r04), which slowly releases the radical R[•] (**IV**) (r05, b05 = 12.5 Kcal/mol) (Table 3 and Scheme 4). R[•] can dimerize

(r06) or reacts mainly with TiCl_3THF complex (r08) instead of interacting with free TiCl_3 (r07). Reaction r08 competes favourably with r06 due to the high $\text{TiCl}_3\text{THF}/\text{R}'$ concentration ratio. Finally, the product R-H is mostly formed through r09, rather than by the alternative r10, because the TiCl_3OH concentration is higher than that of HCl . According to the simulation (Table 1, entry 5 conditions) the formation of HCl is energetically feasible through a $(\text{TiCl}_3)_2\text{OH}$ complex (r12, r13, Table 3) and HCl removal favours the forward flux through these two reversible sequential reactions, thus switching the TiCl_3THF flux from r08 to r12. Then, R' cannot proceed through r08 and it all ends up as its dimer.



Scheme 3. Simplified reaction set simulated with COPASI.



^aRelative energies B3LYP/6-31+G(d,p) scrf = (smd, solvent = THF) // B3LYP/6-31+G(d,p) in Kcal/mol. Selected distances in TS's are shown in Å; R = dimethylallyl.

Scheme 4. Simplified reaction diagram showing the key steps in the mechanism involved in the Ti(III)-mediated deoxygenation of dimethylallyl alcohol (**1b**).^a

Regarding the correlation of experimental and theoretical results, Fig. 2 shows a comparison between the experimental and simulated yields of R–H versus R–R for entries 1, 7, 8, 9 and 5 of Table 1. These entries are ordered by decreasing proportions of TiCl_4 and Mn, except for entry 5 which has the same concentrations as entry 8 but the HCl gas generated is removed from the reaction media. As it can be seen, the agreement between the experimental and theoretical data is remarkable.

Besides, the parameter optimization with Copasi was done using only entries 1, 7, 8 and 9 with the complete reaction diagram.¹⁴ Subsequently, the behaviour for entry 5 (HCl removal) is correctly predicted by the simulator, accounting for the mechanisms described before. This reinforces the consistency of the mechanistic proposals presented herein.

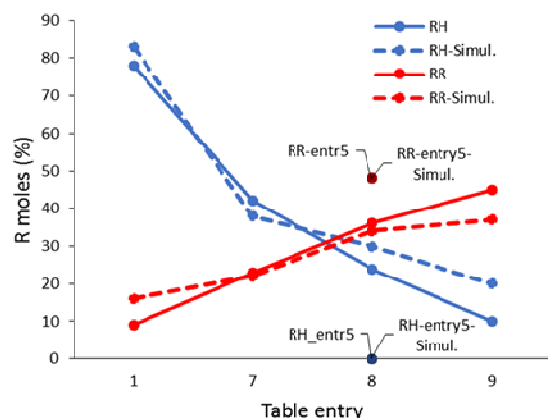


Fig. 2. Experimental and theoretical yields for entries 1, 5, 7, 8 and 9 of Table 1. Entry 5 corresponds to the same experimental conditions as entry 8, but with HCl gas removal.

The complete system of differential equations (Table 3) is solved numerically by Copasi using the optimized barriers listed in it, and the TiCl_4 , Mn initial concentrations (per mol of R–OH) given in Table 1. Thus, for example for entry 7 of Table 1, we get the time evolution for some representative species as represented in Fig. 3. Species not plotted are below 0.02 mol except for THF, Mn, $(\text{TiCl}_3)_2\text{O}$ (almost equal to R–H) and TiCl_3OH (almost equal to R–R). Bearing in mind Scheme 3 (Simplified Reaction Diagram) and Fig. 3, it is noticeable that when the process starts and before R–OH is added (first 30 minutes), TiCl_4 and Mn concentration decrease while forming MnCl_2 and TiCl_3 . However, TiCl_3 is immediately solvated to TiCl_3THF (Fig. 3, green solid line). After 30 minutes of reaction, R–OH is added and interacts slowly (non-negligible forward and reverse barriers b_{03} , b_{03r} , Table 3) with TiCl_3THF to release R' and TiCl_3OH . R' proceeds immediately through r_{08} , r_{09} to form R–H while TiCl_3OH is partially spent to protonate R' through r_{09} . For this particular conditions (Table 1, entry 7; Fig. 3) the reaction stops because all the TiCl_3THF (and TiCl_4) available has been consumed. Reactions r_{12} and r_{13} have a negligible contribution and can also be deleted from the Simplified Reaction Diagram (Scheme 3) except when the generated HCl is removed from the media (Table 1, entry 5).

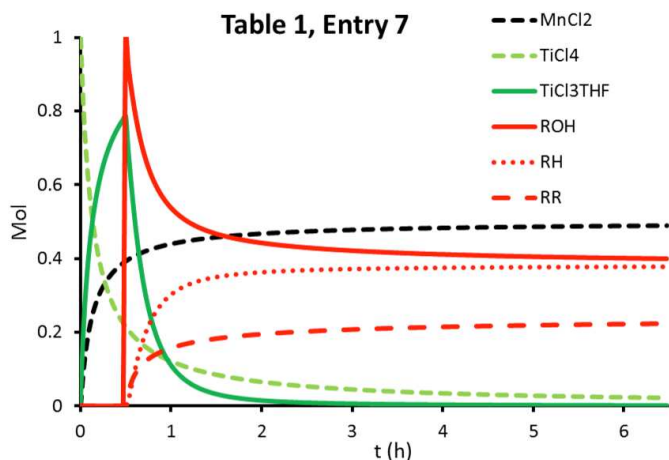


Fig. 3. Simulation of the process for entry 7 of Table 1.

Regarding the role of the kinetics simulator in this *ab-initio* plus *kinetics* simulation approach, the Gaussian calculation is used to provide the set of initial guesses for the barriers. Then the kinetics simulator Copasi is used to fine tune them (within the parameter basins provided by Gaussian) by optimizing the fit to experimental data. It should be stressed that, in this methodology, Copasi is not being used to find the parameter set (which is heavily underdetermined in the present case). This task is assigned to Gaussian, which provides guidance as to whether a reaction path should be considered or not, discarding those with high reaction barriers. Then, the reaction kinetics simulator verifies the feasibility of the presumed outcomes, taking into account not only the barriers but also the concentrations available for each reaction at any given time. For instance, TiCl_3 can be consumed through r_{01} and r_{02} , both with zero forward barrier, but the simulation shows a negligible flow through r_{02} due to concentration effects, as discussed before. In addition, since the model is built on physically-based mechanisms, it is likely to have more robust prediction capabilities, like the HCl gas removal effect, which was not considered as input in the parameter optimization and yet is correctly predicted as a result of the proposed mechanisms.

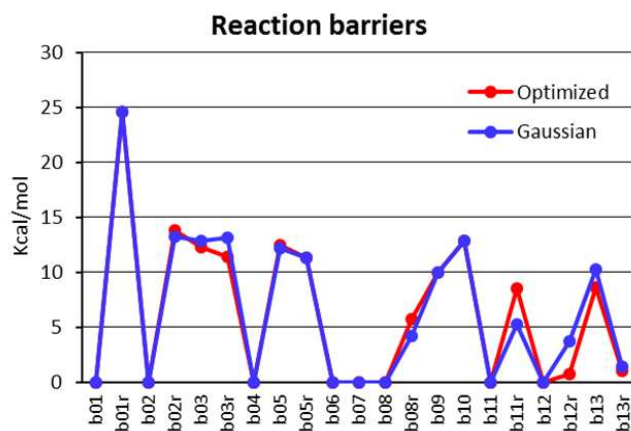


Fig. 4. Graph showing a comparison between the barrier values obtained with Gaussian09 and optimized with COPASI.

Conclusion

In conclusion, in this work strong evidence is provided to support that activated (allylic or benzylic) alcohols give rise to deoxygenation-reduction reactions with excess Ti(III) in refluxing THF via homolysis to radicals. These key intermediates develop into organo-Ti species which are subsequently protonated by the Brønsted acids originated in the reaction medium from the H atom of the -OH group. Furthermore it was shown that the corresponding lithium alkoxides and the alcohols themselves can be involved in dimerization reactions by using equimolecular quantities of Ti(III). An ab-initio plus kinetics simulation approach was used to model and analyse the intervening set of reactions, where the ab-initio calculation provides the reaction barriers and the kinetics simulation reveals the feasibility of the outcomes taking into account the effect of concentrations available for each reaction at any given time. The combined approach seems to be especially useful when there are competing reactions, like the cases presented here. In addition, since the model is built on physically-based mechanisms, it is likely to have more robust prediction capabilities that could allow help design further experiments.

Experimental

General Experimental

The solvents used were purified according to standard literature techniques and stored under Argon. THF was freshly distilled immediately prior to use from sodium/benzophenone and strictly deoxygenated for 30 min under Argon for each of the Cp₂TiCl₂/Mn reactions. Reagents were purchased at the higher commercial quality and used without further purification, unless otherwise stated. Yields refer to chromatographically and spectroscopically (¹H NMR) homogeneous materials, unless otherwise stated. NMR spectra were performed on either a Bruker AV400 or Bruker AV600 spectrometer operating at 400 and 500 MHz respectively for proton and 100 and 125 MHz respectively for carbon nuclei. Chemical shifts (δ) are expressed in parts per million (ppm) and are referenced to residual solvent signal as the internal standard. The accurate mass determination was carried out with an AutoSpec-Q mass spectrometer arranged in an EBE geometry and equipped with a FAB (LSIMS) source. The instrument was operated at 8 KV of accelerating voltage and Cs⁺ were used as primary ions. Silica gel (35–70 μm) was used for flash column chromatography. Reactions were monitored by thin layer chromatography (TLC) carried out on 0.25 mm silica gel plates (60F–254) using UV light as the visualizing agent and solutions of phosphomolybdic acid in ethanol or acidic mixture of anisaldehyde and heat as developing agents. All air- and water-sensitive reactions were performed in flasks flame-dried under a positive flow of Argon and conducted under an Argon atmosphere.

General reduction/homocoupling procedure: Rigorously dry and deoxygenated THF (4.0 mL) was added to a mixture of Cp₂TiCl₂ (2.0 mmol), and Mn dust (8.0 mmol) under an Ar atmosphere and the suspension was stirred at RT until it turned dark green (about 15 min). A solution of **1** (1.0 mmol) in THF (1.0 mL) was then added and the complete reaction mixture refluxed. The mixture was stirred for 2 h and then diluted with *t*-BuOMe and washed with 10% aqueous HCl solution and brine. The organic phase was dried over anhydrous Na₂SO₄ and the solvent was removed in vacuo. The resulting crude was

purified by flash chromatography (*t*-BuOMe/hexane, 4:1) on silica gel to afford a fraction corresponding to pure **4** (9% yield, for entry 1 of Table 1) and a second corresponding to the mixture of **2** and **3** (86% yield, for entry 1 of Table 1). At this point, the compounds **2** and **3** could be separated by column chromatography on AgNO₃ (20%)–Si gel using hexane as eluent (78% and 8% yield of **2** and **3** respectively, for entry 1 of Table 1).

(E)-3,7,11-trimethyldodeca-1,6,10-triene (2).³ ¹H NMR (CDCl₃, 500 MHz) δ 5.71 (dd, *J* = 6.9 Hz, 9.7 Hz, 1H)[‡], 5.70 (ddd, *J* = 7.2 Hz, 10.0 Hz, 17.4 Hz, 1H), 5.08–5.14 (m, 2H), 4.98 (bs, 1H)[‡], 4.96 (br d, *J* = 17.4 Hz, 1H), 4.95 (br d, *J* = 9.7 Hz, 1H)[‡], 4.92 (br d, *J* = 10.0 Hz, 1H), 2.19 (s, 1H)[‡], 2.13 (sept, *J* = 7.2 Hz, 1H), 2.05–2.10 (m, 4H), 1.96–2.01 (m, 2H), 1.69 (s, 3H), 1.61 (s, 3H), 1.59 (s, 3H), 1.30–1.36 (m, 2H), 1.00 (d, *J* = 7.0 Hz, 3H), 0.98 (s, 3H)[‡] ppm. ¹³C NMR (CDCl₃, 125 MHz) δ 144.7, 134.8, 131.2, 124.5, 124.4, 112.4, 39.7, 37.3, 36.7, 26.6, 25.7, 25.6, 20.1, 17.6, 15.9 ppm. HRFABMS calcd. for C₁₅H₂₆Na [M + Na]⁺ 229.1932, found 229.1930. ([‡] Signals corresponding to deuterated derivative).

(6E,10E)-2,6,10-trimethyldodeca-2,6,10-triene (3).³ ¹H NMR (CDCl₃, 400 MHz) δ 5.22 (q, *J* = 7.0 Hz, 1 H), 5.11 (m, 2H), 2.15–2.04 (m, 4H), 2.10–1.95 (m, 4H), 1.68 (s, 3H), 1.61 (s, 9H), 1.57 (d, *J* = 7.0 Hz, 3H) ppm. ¹³C NMR (CDCl₃, 100 MHz) δ 135.7, 134.9, 131.2, 124.4, 124.3, 118.2, 39.7, 39.7, 26.7, 26.6, 25.7, 17.7, 15.9, 15.6, 13.3 ppm. HRFABMS calcd. for C₁₅H₂₆Na [M + Na]⁺ 229.1932, found 229.1928.

(6E,10E,14E,18E)-2,6,10,15,19,23-hexamethyltetracos-2,6,10,14,18,22-hexaene (4).³ ¹H NMR (CDCl₃, 400 MHz) δ 5.17–5.03 (m, 6H), 2.10–1.90 (m, 20H), 1.67 (s, 6H), 1.58 (s, 18H) ppm. ¹³C NMR (CDCl₃, 100 MHz) δ 135.2, 135.0, 131.3, 124.5, 124.4, 124.3, 39.8, 28.3, 26.8, 26.7, 25.8, 17.8, 16.1 ppm. HRFABMS calcd. for C₃₀H₅₀Na [M + Na]⁺ 433.3811, found 433.3813.

Reduction/homocoupling procedure for 5: To a rigorously dry and deoxygenated THF (1.0 mL) solution of **1** (1.0 mmol) was added *tert*-butyllithium in heptane (1.7 M, 0.8 mL) at –78 °C in a two-neck flask, and the mixture was stirred for 20 minutes at room temperature. The solution was turned intense yellow and was evaporated under vacuum. At this point the residue was diluted in THF (5.0 mL) and was added to a green solution of Cp₂TiCl₂ (2.0 mmol) and Mn (8.0 mmol) and refluxed. The reaction mixture was stirred for 2 hours and subsequently diluted with *t*-BuOMe and washed with aq. 1N HCl, saturated NaHCO₃ and brine. The organic phase was dried over anhydrous Na₂SO₄ and the solvent was removed in vacuo. The residue was purified by flash chromatography as described above.

1,2,3-trimethoxy-5-methylbenzene (9).^{5c} According to the general experimental procedure described above, a 91% yield of **9** was obtained after purification of the reaction crude by column chromatography (hexane/*t*-BuOMe, 3:1). ¹H NMR (CDCl₃, 500 MHz) δ 6.37 (s, 2H), 3.82 (s, 6H), 3.80 (s, 3H), 2.29 (s, 3H), 2.27 (m, 2H)[‡] ppm. ¹³C NMR (CDCl₃, 125 MHz) δ 153.0, 137.3, 133.5, 106.0, 60.8, 56.0, 21.5 ppm. HRFABMS calcd. for C₁₀H₁₄O₃Na [M + Na]⁺ 205.0841, found 205.0835. ([‡] Signals corresponding to deuterated derivative).

1,2-bis(3,4,5-trimethoxyphenyl)ethane (10).^{5c} ¹H NMR (CDCl₃, 500 MHz) δ 6.37 (s, 4H), 3.82 (s, 9H), 2.85 (s, 4H) ppm. ¹³C NMR (CDCl₃, 125 MHz) δ 153.1, 137.4, 136.3, 105.5, 61.0, 56.1, 38.6 ppm. HRFABMS calcd. for C₂₀H₂₆O₆Na [M + Na]⁺ 385.1627, found 385.1629.

Reduction/homocoupling procedure for 11. Lithium derivative **11** was prepared, reacted and the resulting crude

purified following similar experimental procedure as for compound **5**.

Results corresponding to experiments carried out for the study and optimization of the reduction/homocoupling methodology (Tables 1–2) were calculated by reaction yields and ¹H NMR integrals in the case of the mixture of **2–3** or **9–10** obtained from the first silica gel flash chromatography.

Theoretical Calculations

Geometry optimizations and energy calculations were performed with GAUSSIAN 09 using DFT at the B3LYP/6-31+G(d,p) level of theory *in vacuo*. To simulate the solvent effect used in the experimental reactions (THF), a single point calculation was performed at the same level described before, using the SMD continuum model. Transition state structures were optimized as saddle points at the same level of calculation. A vibrational analysis was performed at the same level of theory in order to determine the zero-point vibrational energy and to characterize each stationary point as a minimum or transition state structure. Transition states were identified by the presence of a single imaginary frequency that corresponds to the expected motion along the reaction coordinate. The reported energies are expressed in Hartrees (au) and include zero-point energy corrections. The same energies expressed in Kcal/mol as relative energies appear in the Scheme 4 in the paper. To verify that the TSs correspond to the expected reactant and product wells, intrinsic reaction coordinate (IRC) calculations were performed at the same level b3lyp/6-31+g(d,p). In the IRC plots, energies do not include zero point energy corrections. Structural drawings were produced by Spartan'08. Conformational studies were performed using MMFF94 force-field with Spartan 08 previous to quantum mechanical optimization.

The reaction set listed in Table 3 and shown in the Reaction Diagram above was implemented in Copasi (Complex Pathway Simulator). The kinetics of a chemical species is determined by the rate law associated with individual reactions. For example, the concentration of R–H evolves with time as (see Reaction Diagram and r09, r10 in Table 3):

$$d[\text{RH}]/dt = k_{09}[\text{TiCl}_3\text{R}][\text{TiCl}_3\text{OH}] + k_{10}[\text{TiCl}_3\text{R}][\text{HCl}]$$

with $k_{09} = A \cdot \exp(-b_{09}/RT)$, $k_{10} = A \cdot \exp(-b_{10}/RT)$ and $A = 4 \cdot 10^7 \text{ M}^{-1}\text{s}^{-1}$.

Acknowledgements

This project was supported by the Spanish Ministry of Economy and Competitiveness (project CTQ2010-16818-BQ) and Consej. Educ. JCyL, (project SA221U13).

Notes and references

^aDepartment of Organic Chemistry and Institute of Biotechnology, University of Granada, Avda. Fuentenuueva s/n, 18071 Granada, Spain.

^bCIQSO–Center for Research in Sustainable Chemistry, and Department of Chemical Engineering, Physical Chemistry and Organic Chemistry, University of Huelva, Campus el Carmen, 21071 Huelva, Spain.

^cDepartment of Electronics, ETSIT, University of Valladolid, Paseo de Belén 15, 47011, Valladolid, Spain.

^dDepartment of Pharmaceutical Chemistry-IBSAL-CIETUS, University of Salamanca, Avda. Campo Charro s/n, 37071 Salamanca, Spain.

† Electronic Supplementary Information (ESI) available: Text, figures, and tables giving computational methods and ¹H and ¹³C NMR spectra of deuterated derivatives of **2** and **9**. See DOI: 10.1039/b000000x/

- The single electron transfer bis(cyclopentadienyl)-Ti(III) chloride, can be generated *in situ* by stirring commercial Cp₂TiCl₂ with dust Mn. For pioneering reports on the use of this reagent, see: T. V. RajanBabu and W. A. Nugent, *J. Am. Chem. Soc.*, 1994, **116**, 986–997 and references cited therein. For pertinent reviews on the use of this reagent, see (a) A. Gansäuer and H. Bluhm, *Chem. Rev.*, 2000, **100**, 2771–2788; (b) A. Gansäuer, T. Lauterbach and S. Narayan, *Angew. Chem., Int. Ed.*, 2003, **42**, 5556–5573; (c) A. F. Barrero, J. F. Quílez, E. M. Sánchez and J. F. Arteaga, *Eur. J. Org. Chem.*, **2006**, 1627–1641; (d) J. Justicia, L. Álvarez de Cienfuegos, A. Campaña, D. Miguel, V. Jakoby, A. Gansäuer and J. M. Cuerva, *Chem. Soc. Rev.* 2011, **40**, 3525–3537; (e) B. Rossi, S. Prosperini, N. Pastori, A. Clerici and C. Punta, *Molecules*, 2012, **17**, 14700–14732.
- (a) B. Giese, in *Radicals in Organic Synthesis: Formation of Carbon–Carbon Bonds*, Pergamon Press: Oxford, 1986; (b) D. P. Curran, N. A. Porter and B. Giese, in *Stereochemistry of Radical Reactions*, VCH: Weinheim, 1996; (c) D. P. Curran and D. M. Rakiewicz, *J. Am. Chem. Soc.*, 1985, **107**, 1448–1449; (d) S. L. Danishefsky and J. S. Panek, *J. Am. Chem. Soc.*, 1987, **109**, 917–918.
- H. R. Diéguez, A. López, V. Domingo, J. F. Arteaga, J. A. Dobado, M. M. Herrador, J. F. Quílez and A. F.; Barrero, *J. Am. Chem. Soc.*, 2010, **132**, 254–259.
- A. Millán, A. Campaña, B. Bazdi, D. Miguel, L. Álvarez de Cienfuegos, A. M. Echavarren and J. M. Cuerva, *Chem. Eur. J.*, 2011, **17**, 3985–3994.
- (a) A. F. Barrero, M. M. Herrador, J. F. Quílez, P. Arteaga, J. F. Arteaga, H. R. Diéguez and E. M. Sánchez, *J. Org. Chem.*, 2007, **72**, 2988–2995; (b) A. F. Barrero, M. M. Herrador, J. F. Quílez, P. Arteaga, J. F. Arteaga, M. Piedra and E. M.; Sánchez, *Org. Lett.*, 2005, **7**, 2301–2304; (c) A. F. Barrero, M. M. Herrador, J. F. Quílez, P. Arteaga, M. Akissira, F. El Hanbali, J. F. Arteaga, H. R. Diéguez and E. M. Sánchez, *J. Org. Chem.*, 2007, **72**, 2251–2254.
- A. F. Barrero, J. F. Quílez, E. M. Sánchez and J. F. Arteaga, *Org. Lett.*, 2006, **8**, 667–672.
- J. S. Yadav, T. Shekharm and V. R. Gadgil, *J. Chem. Soc., Chem. Commun.*, 1990, **11**, 843–844.
- The options are (i) Cp₂TiClOH generated according to path–B in Scheme 1; (ii) HCl formed by elimination during the process, or (iii) the H₂O present in the work-up of the reaction.
- GAUSSIAN09 (Frisch, M. J., et al., Revision B.01, Gaussian, Inc., Pittsburgh, PA, **2010**). M. J. Frisch, G. W. Trucks, H. B. Schlegel, G. E. Scuseria, M. A. Robb, J. R. Cheeseman, G. Scalmani, V. Barone, B. Mennucci, G. A. Petersson, H. Nakatsuji, M. Caricato, X. Li, H. P. Hratchian, A. F. Izmaylov, J. Bloino, G. Zheng, J. L. Sonnenberg, M. Hada, M. Ehara, K. Toyota, R. Fukuda, J. Hasegawa, M. Ishida, T. Nakajima, Y. Honda, O. Kitao, H. Nakai, T. Vreven, J. A. Montgomery, Jr., J. E. Peralta, F. Ogliaro, M. Bearpark, J. J. Heyd, E. Brothers, K. N. Kudin, V. N. Staroverov, R. Kobayashi, J. Normand, K. Raghavachari, A. Rendell, J. C. Burant, S. S. Iyengar, J. Tomasi, M. Cossi, N. Rega, J. M. Millam, M. Klene, J. E. Knox, J. B. Cross, V. Bakken, C. Adamo, J. Jaramillo, R. Gomperts, R. E. Stratmann, O. Yazyev, A. J. Austin, R. Cammi, C. Pomelli, J. W. Ochterski, R. L.

- Martin, K. Morokuma, V. G. Zakrzewski, G. A. Voth, P. Salvador, J. J. Dannenberg, S. Dapprich, A. D. Daniels, O. Farkas, J. B. Foresman, J. V. Ortiz, J. Cioslowski, D. J. Fox in Gaussian 09, Revision B.01, Vol. Gaussian, Inc., Wallingford, CT, 2009.
- 10 (a) A. D. Becke, *J. Chem. Phys.*, 1993, **98**, 5648–5652; (b) A. D. Becke, *J. Chem. Phys.*, 1993, **98**, 1372–1377; (c) M. J. Frisch, *J. Phys. Chem.*, 1994, **98**, 11623–11627.
- 11 (a) F. Himo and P. E. M. Siegbahn, *Chem. Rev.*, 2003, **103**, 2421–2456; (b) A. D. Becke, *J. Chem. Phys.*, 1993, **98**, 1372–1377.
- 12 (a) A. Clerici, L. Clerici and O. Porta, *Tetrahedron Lett.*, 1996, **37**, 3035–3038; (b) A. Clerici and O. Porta, *Tetrahedron Lett.*, 1982, **23**, 3517–3520; (c) A. Clerici and O. Porta, *J. Org. Chem.*, 1985, **50**, 76–81.
- 13 A. Gansäuer, K. Knebel, C. Kube, M. van Gastel, A. Cangönül, K. Daasbjerg, T. Hangele, M. Hülsen, M. Dolg and J. Friedrich, *Chem. Eur. J.* 2012, **18**, 2591–2599.
- 14 See SI, sections 3.4.2 (Structure, Cartesian Coordinates and Energies of $T_{S_{I-VII}}$) and 3.4.3 (Plot of IRC_{I-VII}).
- 15 See the complete reaction diagram in Scheme 1a, section 3.1.1 of the SI.
- 16 COPASI 4.10, from <http://www.copasi.org>. S. Hoops, S. Sahle, R. Gauges, C. Lee, J. Pahle, N. Simus, M. Singhal, L. Xu, P. Mendes and U. Kummer, *Bioinformatics*, 2006, **22**, 3067–3074.
- 17 For other examples of systems modelled with Copasi see: (a) D. A. Colby, R. G. Bergman and J. A. Ellman, *J. Am. Chem. Soc.*, 2008, **130**, 3645–3651; (b) M. P. Watson, L. E. Overman and R. G. Bergman, *J. Am. Chem. Soc.*, 2007, **129**, 5031–5044; (c) R. Ghosh, X. Zhang, P. Achord, T. J. Emge, K. Krogh-Jespersen and A. S. Goldman, *J. Am. Chem. Soc.*, 2007, **129**, 853–866.
- 18 R. J. Enmaerke, J. Larsen, T. Skrydstrup and K. Daasbjerg, *J. Am. Chem. Soc.*, 2004, **126**, 7853–7864.